



# Accumulation rates and chronologies from depth profiles of $^{210}\text{Pb}_{\text{ex}}$ and $^{137}\text{Cs}$ in sediments of northern Beibu Gulf, South China sea

Jing Guo<sup>a,b,c,d</sup>, Ozeas S. Costa Jr.<sup>d</sup>, Yinghui Wang<sup>a,b,\*</sup>, Wuhui Lin<sup>a,b</sup>, Shaopeng Wang<sup>a,b</sup>, Bo Zhang<sup>a,b</sup>, Yefeng Cui<sup>a,b</sup>, Hao Fu<sup>a,b</sup>, Linlin Zhang<sup>a,b</sup>

<sup>a</sup> Guangxi Laboratory on the Study of Coral Reefs in the South China Sea, Nanning, 530004, China

<sup>b</sup> School of Marine Sciences, Guangxi University, Nanning, 530004, China

<sup>c</sup> College of Civil Engineering and Architecture, Guangxi University, Nanning, 530004, China

<sup>d</sup> School of Earth Sciences, The Ohio State University at Mansfield, Mansfield, OH, 44906, USA

## ARTICLE INFO

### Keywords:

Geochronology  
Radiotracers  
Sedimentation rates  
Beibu Gulf  
South China sea

## ABSTRACT

Beibu Gulf is a highly dynamic and complex coastal environment that is currently experiencing one of the largest rates of development and urbanization in west China. Little is known about the effects of this increased human activity on coastal sedimentation processes and on the rates of sediment accumulation and the variation of organic materials to the coast. In this study, four sediment cores were collected and applied the  $^{210}\text{Pb}$  dating method to reconstruct sedimentation rates and historical changes of materials to the northern Beibu Gulf over the past century. Depth profiles of excess  $^{210}\text{Pb}$  ( $^{210}\text{Pb}_{\text{ex}}$ ) showed highest activity values at the surface ( $28.4\text{--}104.0\text{ Bq kg}^{-1}$ ) followed by a linear or exponential decay with depth for all but one study site.  $^{137}\text{Cs}$  activity ranged between  $0.236$  and  $2.034\text{ Bq kg}^{-1}$ , and a distinct peak activity – representing the 1963 fallout maximum – was observed at all but one site. Sediment chronologies were determined using the Constant Rate of Supply (CRS) model. Calculated accumulation rates in the studied sites were the lowest in the late 1920s and early 1930s (mass accumulation rate (MAR):  $0.06 \pm 0.01\text{ g cm}^{-2}\text{ y}^{-1}$ ; sediment accumulation rate (SAR):  $0.08 \pm 0.01\text{ cm y}^{-1}$ ) and increased gradually until reaching maximum values in the 2010s (MAR:  $0.22 \pm 0.09\text{ g cm}^{-2}\text{ y}^{-1}$ ; SAR:  $0.46 \pm 0.32\text{ cm y}^{-1}$ ). Current accumulation rates are up to 800% higher than rates observed in the 1920s, with most of the increase happening after 1970, coinciding with the increasing rate of urbanization and development in the region. The highest increase in SAR over the last century (+877%) was observed in Sanniang Bay, with the lowest rate of increase (+283%) observed in Lianzhou Bay. TOC content in these sediments has also increased over the last 100 years. Current values (0.98–1.28%) are about 170% higher than historical concentrations (before 1970). The positive correlations between TOC and population density and GDP growth in major cities surrounding the gulf, provide further indication that human activities have significantly altered the sedimentary environment in recent decades along the northern Beibu Gulf coast.

## 1. Introduction

Sediments in marine ecosystems are repositories of environmental change and can provide historical trends of various elements or contaminants induced naturally and anthropogenically. It can also give valuable information on special historical events and may assist in reconstructing local paleoclimatic conditions (Appleby, 2001; Oldfield et al., 2003; Lüder et al., 2006; Di Gregorio et al., 2007). In coastal ecosystems, which are particularly sensitive to the processes occurring in their estuarine areas, information stored in the sediments is a reliable

tool for investigating the natural and anthropogenic changes in the local environment. Therefore, estimating the accumulation rates and chronologies of coastal sediments is crucial to study the contamination history of these ecosystems. Our targeted area, northern Beibu Gulf, is a typical example of a coastal area influenced by the complex interplay between natural processes and human activities. It is not only the most unique coastal area of west China, but also an important maritime transportation hub for the ASEAN-China Free Trade Area, the largest free trade area based on population, and the third largest based on nominal GDP (Li et al., 2015). Consequently, the coastal regions of

\* Corresponding author. Guangxi Laboratory on the Study of Coral Reefs in the South China Sea, Nanning, 530004, China.

E-mail address: [wyh@gxu.edu.cn](mailto:wyh@gxu.edu.cn) (Y. Wang).

<https://doi.org/10.1016/j.jenvrad.2019.106136>

Received 25 May 2019; Received in revised form 28 September 2019; Accepted 9 December 2019

Available online 15 December 2019

0265-931X/© 2019 Published by Elsevier Ltd.

northern Beibu Gulf have been subjected to high loading of anthropogenic contaminants from agriculture and from domestic and industrial wastewater, resulting from rapid coastal development and urbanization (Kaiser et al., 2013).

Previous studies have used natural radionuclides for determining the accumulation rates and chronologies of sediment deposition in coastal areas. Due to its half-life of about 22.3 years,  $^{210}\text{Pb}$  has proved to be an important nuclide for studying coastal sedimentary processes (Appleby, 2001; Mahmood et al., 2011; Sanchez-Cabeza and Ruiz-Fernández, 2012; Venunathan and Narayana, 2016; Delbono et al., 2016). Since  $^{210}\text{Pb}$  has a short residence time in the atmosphere, it is quickly sequestered in sediments and, over just a few months, it becomes permanently fixed onto sediment particles (Tee et al., 2003). This radionuclide has been widely used to establish continuous chronologies of sedimentation rates and contaminant loadings for a dating horizon of about seven half-lives, i.e., between 120 and 150 years (Kirchner, 2011; Corcoran et al., 2018). The  $^{210}\text{Pb}$  technique was first applied by Koide et al. (1972) to date marine sediments. Determining the sedimentation rates and sediment chronology commonly involves three classical models, which are described in detail by Arias-Ortiz et al. (2018): (1) the constant initial concentration (CIC) model; (2) the constant rate of supply (CRS) model and (3) the constant flux constant sedimentation (CFCS) model. Since each model has specific assumptions based on different environmental conditions, the selection of models should take into account the sedimentation processes in each aquatic ecosystem. One important assumption of all these models is that there is no post-depositional mobility of  $^{210}\text{Pb}$ . In addition, use of  $^{210}\text{Pb}$  dating models should be validated with at least one independent tracer, which separately provides a clear time-stratigraphic horizon (Smith, 2001; Appleby, 2008). The radionuclide  $^{137}\text{Cs}$  is a well-known chronostratigraphic marker that provides the support horizon from distinct and well-defined atmospheric sources, namely the testing of nuclear weapons in the 1950s–1960s, in particular the 1963 fallout maximum. These records of weapons test fallout have long been used to identify the depth of sediments deposited during those years (Klaminder et al., 2012). More recently, records of the nuclear reactor accident in Chernobyl (April 1986) have also been used to identify the depth dated as 1986 in sediments (Egorov et al., 1999; Appleby, 2001; Sari et al., 2018). This method of  $^{137}\text{Cs}$  dating has become increasingly important as a complementary tool to  $^{210}\text{Pb}$  dating when establishing age depth models in recent sedimentary deposits (Appleby, 2001; Sanders et al., 2006; Kumar et al., 2007; Smol, 2008; Sari et al., 2018).

In this study, we provide the first record of sediment accumulation rates and chronologies for the northwestern portion of the South China Sea. We employed the CIC, CRS and CFCS models to estimate the depositional chronologies and determined the optimum model by support with the  $^{137}\text{Cs}$  tracer. This result establishes the baseline of sedimentation rates in northern Beibu Gulf and will support future studies of erosion, sedimentation, and sediment contamination in this region.

## 2. Materials and methods

### 2.1. Study site

Beibu Gulf is located in the northwest corner of the South China Sea, and is surrounded by the country of Vietnam, in the west, and by Leizhou Peninsula, the Qiongzhou Strait, and Hainan Island, in the east (Fig. 1). The northern portion of the gulf extends along the 1628 km of coastline of the Chinese province of Guangxi, covering an area of approximately 129,300 km<sup>2</sup>, from the Beilun River estuary in the west to Tieshan Bay in the east. These coastal waters are shallow, with an average depth of about 10 m (Ma et al., 2010; Xia et al., 2011). The Guangxi coast has a subtropical monsoonal climate, with an annual average rainfall of about 1670 mm. The area is influenced by the East Asian monsoon, with marked dry (November–March) and wet (April–October) seasons. The prevailing wind is mainly south-southwest in summer and north-northeast in winter (Chen et al., 2009).

Sediments are delivered to the coastal zone by five major rivers: The Fangcheng River, which drains into the Fangcheng Bay; the Maoling and Qin rivers, which drain into the Maowei Sea; the Dafeng and Nanliu rivers, which drain into the Lianzhou Bay. Several cities in the Beibu Gulf, such as Nanning, Zhanjiang, Beihai, Fangchenggang, Qinzhou, and Haikou, have experienced rapid development in the past two decades, and the current population living in these cities is estimated to be over 20 million people (Pan et al., 2019).

### 2.2. Sampling procedures and analysis

For this study, sediment cores were collected during August 2017, using a gravity corer with a sampling tube of 100 cm. The corer is 10 cm in diameter and is made of stainless steel. Four cores were sampled (Fig. 1): C1 (located in Qisha Harbor, about 8 km south of the Fangchenggang Nuclear Power Plant, which is currently under construction), C2 (located in Maowei Sea, about 10 km northwest of Longmen Port), C3

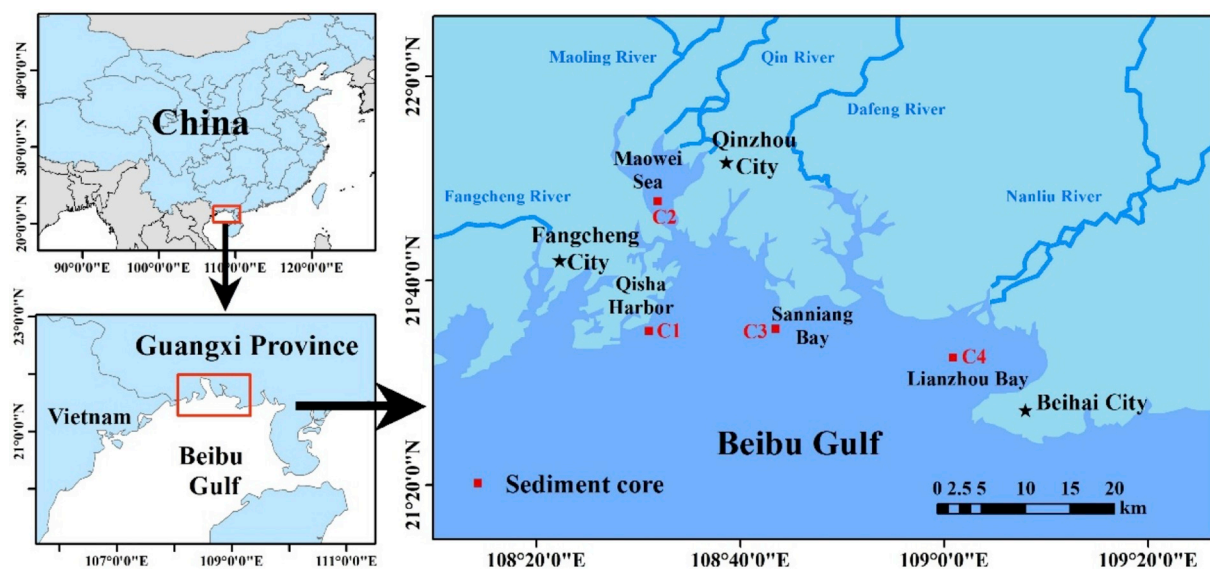


Fig. 1. Map of study area in northern Beibu Gulf and site location of sediment cores.

(located in Sanniang Bay, about 4 km south of Sanniangwan International Dolphins Park), and C4 (located in Lianzhou Bay, about 7 km northwest of the city of Beihai). The cores were maintained in a vertical position throughout sampling in order to avoid any disturbance of the sediment in the coring tubes. A description of the sediment cores is presented in Table 1.

Soon after the corer was brought to the ship's deck, sediment sub-samples were recovered at every 1-cm interval. Wet and dry weights were measured in each sediment sub-sample. These samples were oven-dried at 60 °C for 24 h, and physical parameters, such as water content and wet and dry bulk density, were determined. Particle-size spectra of sediments were measured at 1-cm intervals using an automated laser optical particle-size analyzer after the removal of carbonates by 10% HCl and of organic matter by 30% H<sub>2</sub>O<sub>2</sub> with sodium hexametaphosphate as a dispersing agent. The error on these measurements was lower than 5%. After freeze-drying, grinding, and acidification with 2 N HCl, determination of total organic carbon (TOC) concentrations were performed in the sub-samples using an Elementar® vario MACRO cube elemental analyzer. Sample aliquots used for radionuclide analyses were frozen immediately, and later freeze-dried and pulverized using a mortar and pestle.

For sediment chronology determination, a broad-energy high purity germanium (HPGe)  $\gamma$ -spectrometry (Canberra BE6530, relative efficiency 63.4%) was used to measure <sup>210</sup>Pb (46.5 keV), <sup>137</sup>Cs (661.7 keV) and <sup>226</sup>Ra activity were calculated by the  $\gamma$ -rays of their progenies at the photopeaks of 351.9 keV (<sup>214</sup>Pb/<sup>226</sup>Ra) and 609.3 keV (<sup>214</sup>Bi/<sup>226</sup>Ra) based on the secular equilibrium of radium and its progenies (Lin et al., 2019). This high-resolution gamma spectrometer is equipped with a HPGe type ORTEC GMX detector, having a FWHM of 1.58 keV at 1332 keV and a Be window of 0.5 mm, allowing the detection of low gamma energies. 10 g dry samples were placed in sealed polyethylene tubes and stored for at least one month prior to measurement (as reported in Begy et al., 2018; Chen et al., 2019 and Lin et al., 2019) in order to ensure radioactive equilibrium between <sup>226</sup>Ra and <sup>222</sup>Rn (half-life of 3.8 days). The measuring time of these elements is about 1–2 days. For analytical quality control, the standard sediment of IAEA-385 was analyzed using the relative efficiency derived from the standard river sediment (GBW08304a). The obtained value was consistent with the reference value of IAEA-385 corrected to April 18, 2017. Specific activities and one sigma counting errors were calculated using standard counting techniques (Mook, 2001). Reported activities were corrected for detector background and decay from time of sampling to the starting time of the gamma spectrometry measurement. Limits of quantification for radionuclides were defined as three times the standard deviation of the background under the peak used for the activity quantification. Under conditions of 100 g sediment and a measurement time of 2 days, the minimum detectable activity for <sup>210</sup>Pb, <sup>226</sup>Ra and <sup>137</sup>Cs though Canberra BE6530 was 0.9, 0.8, 0.14, respectively. The uncertainties for <sup>210</sup>Pb, <sup>226</sup>Ra and <sup>137</sup>Cs is 7%, 4%, 10%, respectively.

**Table 1**  
Sampled cores and their characteristics.

Code	Position	Location		Depth	
		N	E	Length (cm)	Water (m)
C1	Qisha Harbor	21° 56'	108° 30'	77	6.2
		59.8''	54.2''		
C2	Maowei Sea	21° 45'	108° 32'	65	3.4
		22.4''	11.6''		
C3	Sanniang Bay	21° 35'	108° 43' 9.3''	70	5.6
		35.1''			
C4	Lianzhou Bay	21° 32'	108° 59'	62	4.3
		10.6''	44.7''		

### 2.3. Sediment chronology models

Our approach was to apply the <sup>210</sup>Pb models uniformly to all sediment cores in order to obtain net apparent mean sediment mass accumulation rates (MAR) and sediment accumulation rate (SAR), and to validate these models using the anthropogenic radionuclide <sup>137</sup>Cs (t<sub>1/2</sub> = 30.08 years) as an independent constraint on sediment age at the 1963 horizon. Here, <sup>210</sup>Pb<sub>ex</sub> was the basic parameter in the following models and it was obtained by subtracting measured <sup>226</sup>Ra activity from the total <sup>210</sup>Pb activity.

#### 2.3.1. CIC model

The CIC model assumes that the initial <sup>210</sup>Pb concentration in the deposited sediment is a constant, regardless of changes in the sediment accumulation rate (Appleby and Oldfield, 1978, 1983). This hypothesis actually means that the <sup>210</sup>Pb<sub>ex</sub> concentration, when one sediment section is formed, is constant, with a value that we denote as C<sub>0</sub>. By using this hypothesis, the date determination can be written as:

$$t_i = \frac{1}{\lambda} \ln \frac{C_0}{C_i} \quad (1)$$

where  $\lambda = (\ln 2)/\text{half-life of } ^{210}\text{Pb} = 0.693/22.26 \text{ yr} = 0.03114 \text{ yr}^{-1}$  is the radioactive decay constant of <sup>210</sup>Pb. C<sub>0</sub> can be obtained from a linear regression fit of lnC<sub>i</sub> versus mass depth (m<sub>i</sub>). The intercept is a = lnC<sub>0</sub> and therefore C<sub>0</sub> = e<sup>a</sup>.

In order to determine the accumulation rate, we need to estimate layer ages. We calculate age means for each layer with the equation: t(i) =  $\frac{t_i + t_{i+1}}{2}$ . The last layer age must be obtained by extrapolation as t(j) = t<sub>j</sub> +  $\frac{t_j - t_{j-1}}{2}$ . Section formation time ( $\Delta t_i$ , yr) is the age difference between two consecutive layers,  $\Delta t_i = t_{i+1} - t_i$ . The mean sediment accumulation rate (S<sub>i</sub>, cm yr<sup>-1</sup>) is the quotient between the section width and its formation time. For section i:  $S_i = \frac{z(i+1) - z(i)}{\Delta t_i}$ . Mean mass accumulation rate (R<sub>i</sub>, g cm<sup>-2</sup> yr<sup>-1</sup>) is given by  $R_i = \frac{m(i+1) - m(i)}{\Delta t_i}$ , where m(i) is the mass depth of layer (i) (kg m<sup>-2</sup>),  $m(i) = \sum_{j=1}^{i-1} \frac{\Delta m_j}{S}$ ,  $\Delta m_i$  is the dry mass of section i (kg).

#### 2.3.2. CRS model

The CRS model assumes that the flux of <sup>210</sup>Pb to the accumulating sediment is constant during a timescale of 100–200 years (Robbins and Edgington, 1975). It is based on the comparison of <sup>210</sup>Pb<sub>ex</sub> inventories below a given depth with the overall <sup>210</sup>Pb<sub>ex</sub> inventory in the sediment core. According to the CRS model, site-specific sediment MAR, SAR and layer age (t<sub>i</sub>) at the depth i could be estimated from the slope of Eq. (2), Eq. (3) and Eq. (4).

$$\text{MAR (g cm}^{-2}\text{yr}^{-1}) = A_i/C_i \times \frac{1}{\lambda} \quad (2)$$

$$\text{SAR (cm yr}^{-1}) = \text{MAR} \times \rho \quad (3)$$

$$t_i = \frac{1}{\lambda} \ln \frac{A_0}{A_i} \quad (4)$$

where A<sub>i</sub> is the accumulated <sup>210</sup>Pb<sub>ex</sub> deposit below layer (i), and C<sub>i</sub> is the <sup>210</sup>Pb<sub>ex</sub> concentration in layer (i).  $\rho$  is the mean dry bulk density of a certain layer.

#### 2.3.3. CFCS model

The CFCS model assumes a constant flux to the sediment surface and constant mass accumulation rate (Appleby and Oldfield, 1983). This means a purely exponential decrease of C<sub>i</sub> with depth should be observed. In order to get the MAR, we can solve the following equation through linear regression (Croaz et al., 1964) between the ln C<sub>i</sub> and the mass depth m<sub>i</sub>:

$$\ln C_i = \ln C_0 - \frac{\lambda}{r} m_i \quad (5)$$

from the regression line equation ( $y = a + bx$ ), the slope is  $b = -\frac{\lambda}{R}$ , then  $R = -\frac{\lambda}{b}$ .

So, the layer age  $t_i$  can be given by

$$t_i = \frac{m_i}{R} \quad (6)$$

### 2.3.4. $^{210}\text{Pb}_{\text{ex}}$ fluxes

$^{210}\text{Pb}_{\text{ex}}$  fluxes can be calculated by the following equation:

$$F \text{ (Bq m}^{-2}\text{yr}^{-1}) = \lambda A / (1 - e^{-\lambda t}) \quad (7)$$

where  $A$  is the total accumulated  $^{210}\text{Pb}_{\text{ex}}$  deposit, and  $t$  is the age of integrated sediment core.

## 3. Results

### 3.1. Depth profiles of $^{210}\text{Pb}_{\text{total}}$ and $^{226}\text{Ra}$ activities

Depth profiles of  $^{210}\text{Pb}_{\text{total}}$  and  $^{226}\text{Ra}$  activities in the sediment cores are shown in Fig. 2.  $^{210}\text{Pb}_{\text{total}}$  activities varied 63.4–141.5  $\text{Bq kg}^{-1}$  in Qisha Harbor (C1), 97.38–133.29  $\text{Bq kg}^{-1}$  in Maowei Sea (C2), 35.6–107.1  $\text{Bq kg}^{-1}$  in Sanniang Bay (C3), and 44.3–84.5  $\text{Bq kg}^{-1}$  in Lianzhou Bay (C4).  $^{210}\text{Pb}_{\text{total}}$  activities showed highest values at the

surface followed by an exponential or linear decay with depth for all but the Maowei Sea (C2) profile. This sediment core showed a stair-stepped profile, with a number of subsurface peaks, and highest activities being observed at depths below 20 cm. In Qisha harbor (C1),  $^{210}\text{Pb}_{\text{total}}$  activity at the top of the profile (0-cm depth) was  $141.5 \pm 7.4 \text{ Bq kg}^{-1}$ , decreasing to  $107.8 \pm 8.6 \text{ Bq kg}^{-1}$  at 13-cm depth, followed by an activity peak ( $118.69 \pm 7.9 \text{ Bq kg}^{-1}$ ) at 18-cm depth. The lowest  $^{210}\text{Pb}_{\text{total}}$  activity at this site ( $63.4 \pm 6.1 \text{ Bq kg}^{-1}$ ) was observed at 70-cm depth. In Sanniang Bay (C3),  $^{210}\text{Pb}_{\text{total}}$  activity at the top of the profile (0-cm depth) was  $107.1 \pm 4.3 \text{ Bq kg}^{-1}$ , decreasing to  $81.6 \pm 6.6 \text{ Bq kg}^{-1}$  at 5-cm depth, followed by an activity peak ( $98.9 \pm 4.7 \text{ Bq kg}^{-1}$ ) at 8-cm depth. The lowest  $^{210}\text{Pb}_{\text{total}}$  activity ( $35.6 \pm 2.2 \text{ Bq kg}^{-1}$ ) was observed at 70-cm depth. In Lianzhou Bay (C4),  $^{210}\text{Pb}_{\text{total}}$  activity at the top of the profile (0-cm depth) was  $84.5 \pm 5.2 \text{ Bq kg}^{-1}$ , decreasing exponentially until reaching the lowest activity ( $44.3 \pm 4.7 \text{ Bq kg}^{-1}$ ) at 60-cm depth.

$^{226}\text{Ra}$  activities were relatively stable, with a mean of  $37.4 \pm 1.1 \text{ Bq kg}^{-1}$  in Qisha Harbor (C1),  $49.7 \pm 4.5 \text{ Bq kg}^{-1}$  in Maowei Sea (C2),  $27.8 \pm 1.6 \text{ Bq kg}^{-1}$  in Sanniang Bay (C3), and  $50.6 \pm 4.1 \text{ Bq kg}^{-1}$  in Lianzhou Bay (C4).  $^{210}\text{Pb}_{\text{total}}$  activity reached a radioactive equilibrium with  $^{226}\text{Ra}$  activity only at the Lianzhou Bay profile, at the 25-cm depth. For the other profiles,  $^{210}\text{Pb}_{\text{total}}$  activity at the bottom of the core was greater than  $^{226}\text{Ra}$  activity at the same depth. For C1, mean  $^{210}\text{Pb}_{\text{total}}$  activity at the 70-cm depth was  $63.4 \text{ Bq kg}^{-1}$ , while mean  $^{226}\text{Ra}$  activity was  $36.4 \text{ Bq kg}^{-1}$ ; For C2, mean  $^{210}\text{Pb}_{\text{total}}$  activity at the 60-cm depth was  $126.5 \text{ Bq kg}^{-1}$ , while mean  $^{226}\text{Ra}$  activity was  $56.5 \text{ Bq kg}^{-1}$ ; For C3, mean  $^{210}\text{Pb}_{\text{total}}$  activity at the 70-cm depth was  $36.1 \text{ Bq kg}^{-1}$ , while mean

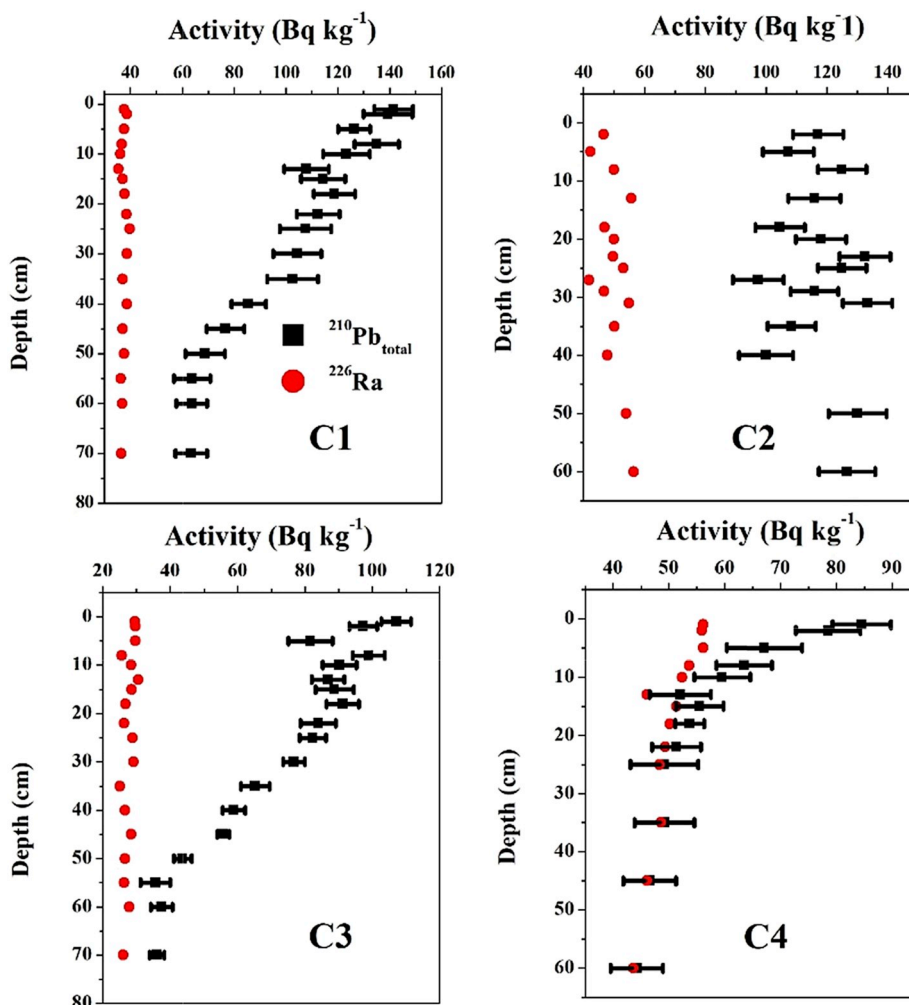


Fig. 2. Depth profiles of  $^{210}\text{Pb}_{\text{total}}$  and  $^{226}\text{Ra}$  in sediment cores.

$^{226}\text{Ra}$  activity was  $26.1 \text{ Bq kg}^{-1}$ .

### 3.2. $^{210}\text{Pb}_{\text{ex}}$ and $^{137}\text{Cs}$ activities

Due to  $^{226}\text{Ra}$  activity being relatively constant, the depth distribution of  $^{210}\text{Pb}_{\text{ex}}$  activity (Fig. 3) was similar to the  $^{210}\text{Pb}_{\text{total}}$  distribution. With the exception of C2, the highest  $^{210}\text{Pb}_{\text{ex}}$  activity was found in the top section of each core:  $104.0 \pm 7.5 \text{ Bq kg}^{-1}$  at C1,  $77.5 \pm 3.4 \text{ Bq kg}^{-1}$  at C3, and  $28.4 \pm 3.1 \text{ Bq kg}^{-1}$  at C4.  $^{210}\text{Pb}_{\text{ex}}$  activity generally decreased exponentially or linear with depth ( $R^2 > 0.9$ ), except for profile C2 in Maowei Sea. According to the fitting curve between  $^{210}\text{Pb}_{\text{ex}}$  and depth, the deepest activities of  $^{210}\text{Pb}_{\text{ex}}$  was estimated. Using equation (7), this estimation yielded  $^{210}\text{Pb}_{\text{ex}}$  fluxes of  $260.25 \text{ Bq m}^{-2} \text{ yr}^{-1}$  in Qisha Harbor (C1),  $181.93 \text{ Bq m}^{-2} \text{ yr}^{-1}$  in Sanniang Bay (C3), and  $20.65 \text{ Bq m}^{-2} \text{ yr}^{-1}$  in Lianzhou Bay (C4).

$^{137}\text{Cs}$  activity was detected with a range between 0.24 and  $2.03 \text{ Bq kg}^{-1}$  (Fig. 3). Except for the irregular profile in Maowei Sea,  $^{137}\text{Cs}$  activity profiles showed a distinct subsurface peak, which is consistent with the history of atmospheric deposition for this radionuclide. In the core from Qisha Harbor, the first detectable  $^{137}\text{Cs}$  activity occurred at 45-cm depth ( $0.76 \text{ Bq kg}^{-1}$ ). The maximum activity value ( $0.99 \text{ Bq kg}^{-1}$ ) was measured at the 40-cm depth.  $^{137}\text{Cs}$  activity then started declining until reaching the lowest value ( $0.21 \text{ Bq kg}^{-1}$ ) at the 5-cm depth. This was followed by another activity peak at the 2-cm depth ( $0.38 \text{ Bq kg}^{-1}$ ). In the core from Sanniang Bay (C3), the first detectable  $^{137}\text{Cs}$  activity also occurred at 45-cm depth ( $1.22 \text{ Bq kg}^{-1}$ ). Similar to the observed at C1, the maximum activity value for C3 ( $2.03 \text{ Bq kg}^{-1}$ ) was also

measured at 40-cm depth, followed by an decline until reaching the lowest value ( $0.24 \text{ Bq kg}^{-1}$ ) at the sediment surface (0-cm depth). Two additional activity peaks were observed in this profile, one at the 25-cm depth ( $1.38 \text{ Bq kg}^{-1}$ ) and another at the 13-cm depth ( $1.06 \text{ Bq kg}^{-1}$ ). In the core from Lianzhou Bay (C4), the first detectable  $^{137}\text{Cs}$  activity occurred at 18-cm depth ( $1.23 \text{ Bq kg}^{-1}$ ). Only one distinct subsurface peak (the maximum  $^{137}\text{Cs}$  activity value) was observed at the 15-cm depth ( $1.81 \text{ Bq kg}^{-1}$ ), followed by an exponential decrease to the sediment surface.

### 3.3. Sediment chronologies and accumulation rates

Calendar dates were estimated using the CIC, CRS and CFCS models, and corroborated with the  $^{137}\text{Cs}$  time marker. Fig. 4 shows the chronologies derived from each of these models for Qisha Harbor (C1), Sanniang Bay (C3), and Lianzhou Bay (C4). Due to the irregular  $^{137}\text{Cs}$  activity profile in Maowei Sea (C2), sediment chronologies were not determined for this location. In C1 and C3, the CIC model generally produced the younger chronologies, while in C4, the CRS model was the one producing the younger chronologies. Support with the  $^{137}\text{Cs}$  time marker suggests that the CRS model is the most suitable for determining chronologies in these profiles. Age estimation based on the CIC model led to a significant time inversion in C3, with the top portion of the profile (above 10-cm depth) having younger ages than the CRS model, while in the bottom portion (below 15-cm depth) the age estimations were older than the CRS model. The CFCS model, on the other hand, produced chronologies for C3 and C4 that were consistently younger

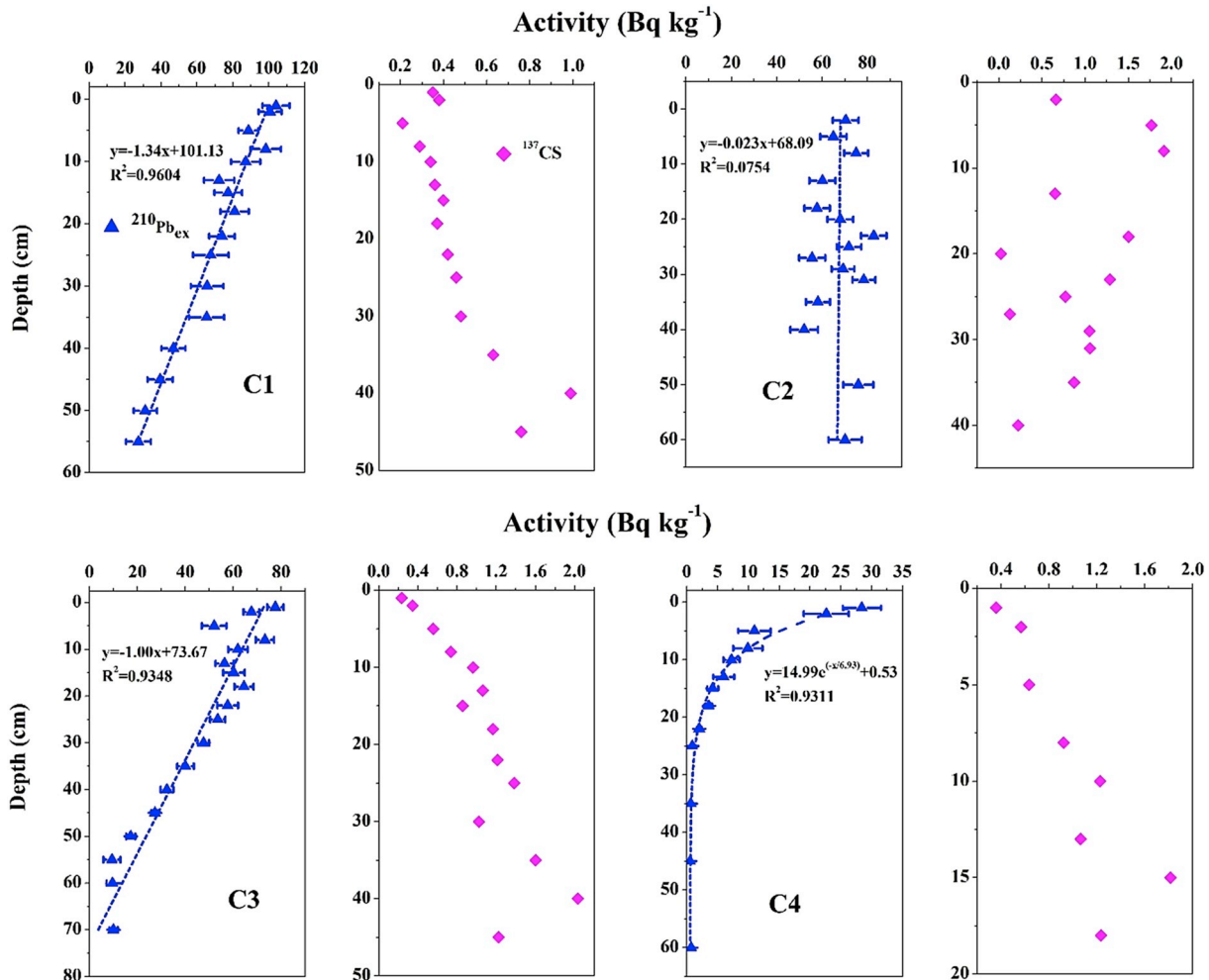


Fig. 3. Depth profiles of  $^{210}\text{Pb}_{\text{ex}}$  and  $^{137}\text{Cs}$  in sediment cores.

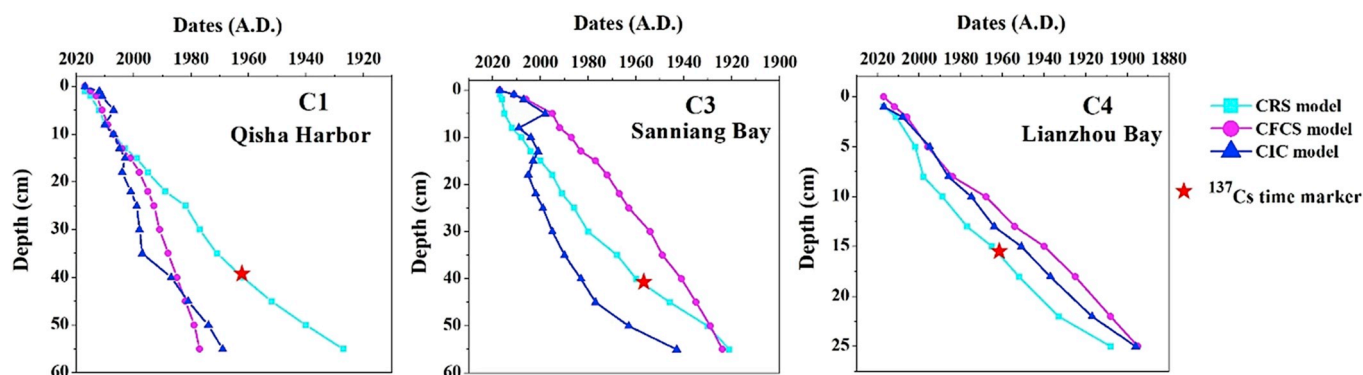


Fig. 4. Chronologies distribution in sediment cores.

than the one provided in the <sup>137</sup>Cs-validated CRS model. For the C1 location, there was good agreement between the age estimations from the CFCS and the CRS models but only in the top 15 cm of the core. Below that depth, age estimations from the CFCS model were consistently older than those produced by the <sup>137</sup>Cs-validated CRS model.

Since the CRS model was the optimum model to estimate the chronologies in our study area, here we show only the MAR and SAR derived from this model. MAR values ranged from 0.05 to 0.24 g cm<sup>-2</sup> y<sup>-1</sup> in Qisha Harbor (C1), from 0.07 to 0.31 g cm<sup>-2</sup> y<sup>-1</sup> in Sanniang Bay (C3), and from 0.07 to 0.12 g cm<sup>-2</sup> y<sup>-1</sup> in Lianzhou Bay (C4). SAR values ranged from 0.09 to 0.43 cm y<sup>-1</sup> in Qisha Harbor, 0.09–0.79 cm y<sup>-1</sup> in Sanniang Bay, and from 0.06 to 0.17 cm y<sup>-1</sup> in Lianzhou Bay. Fig. 5 shows the historical changes in the sedimentation rates in our study sites. In Qisha Harbor, accumulation rates were the lowest in the late 1920s and early 1930s (MAR: 0.05 g cm<sup>-2</sup> y<sup>-1</sup>; SAR: 0.09 cm y<sup>-1</sup>) and increased gradually until reaching maximum values in the 2010s (MAR: 0.24 g cm<sup>-2</sup> y<sup>-1</sup>; SAR: 0.43 cm y<sup>-1</sup>). In Sanniang Bay, accumulation rates declined during the 1920s and remained low (MAR: 0.07 g cm<sup>-2</sup> y<sup>-1</sup>; SAR: 0.09 cm y<sup>-1</sup>) from the late 1920s through most of the 1940s. Accumulation rates then began increasing gradually until reaching maximum MAR in the early 2010s (0.31 g cm<sup>-2</sup> y<sup>-1</sup>) followed by a sharp decline over the recent years, until reaching the current rate of 0.22 g cm<sup>-2</sup> y<sup>-1</sup>. Sedimentation rates, however, have experienced a sharp increase in the 2010s, rising from a SAR of 0.26 cm y<sup>-1</sup> in the late 2000s to the current maximum of 0.79 cm y<sup>-1</sup>. In Lianzhou Bay (C4), mass accumulation rates were also among the lowest during the 1920s and early 1930s (MAR: 0.07 g cm<sup>-2</sup> y<sup>-1</sup>) followed by a gradual increase until reaching the maximum value in 2000 (MAR: 0.17 g cm<sup>-2</sup> y<sup>-1</sup>). After a sharp decline in the early 2000s, the MAR in this location have

continued to drop, until recently reaching values similar to those observed in the 1920s.

### 3.4. Particle size analysis

Results of the particle size analysis are presented in Fig. 6 as a volume percentage of each grain size fraction (sand, silt, clay). Sediments in Qisha Harbor (C1) and Sanniang Bay (C3) are predominantly silty, with mean percentage of silt grains accounting for 48–71% of the sediment in Qisha Harbor and for 64–91% in Sanniang Bay. Sediments in Lianzhou Bay consist mainly of sand, which accounts for 43–86% of particles on this site. The percentage of sand was higher in the upper strata on all three cores, with the amount of silt increasing with depth. The highest amounts of clay were observed in Qisha Harbor, although this size fraction represented only about 5.1% of particles on this site. Sanniang Bay had even smaller amounts of clay, ranging from a high of 3.8% at the upper strata of the core, to a low of 0.9% at the bottom. The clay fraction was virtually absent from the sediments at Lianzhou Bay, with a maximum amount (1.0%) observed at the 15-cm depth.

Fig. 6 also shows the historical changes in median grain size distribution. For all three sites, median grain size was significantly lower in the lower half of the core, increasing almost two-fold towards the top of the core. In Qisha Harbor, median grain size remained relatively stable – at around 0.32 mm – until about 1970, followed by a steady increase in the dominant grain size until the late 1980s. The period between 1990 and 2017 was characterized by sharp fluctuations in the median grain size between a low of 0.31 mm and a high of 0.48 mm. In Sanniang Bay, median grain size increased steadily from a low of 0.19 mm in the 1920s (bottom of the profile) to a high of 0.29 mm around 2015. In Lianzhou

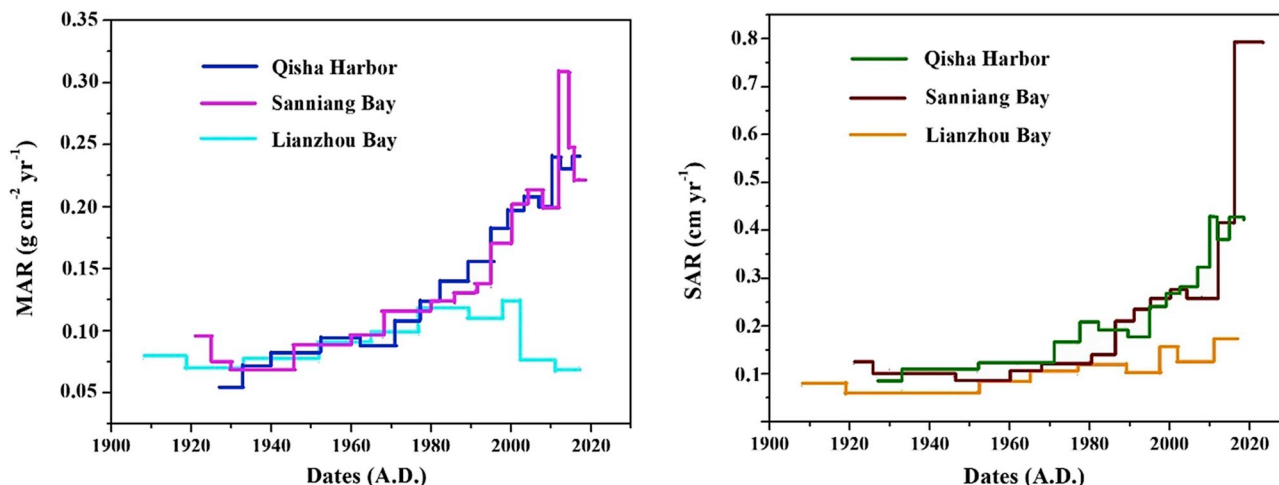


Fig. 5. Historical changes in MAR and SAR derived from the CRS model in the study area.

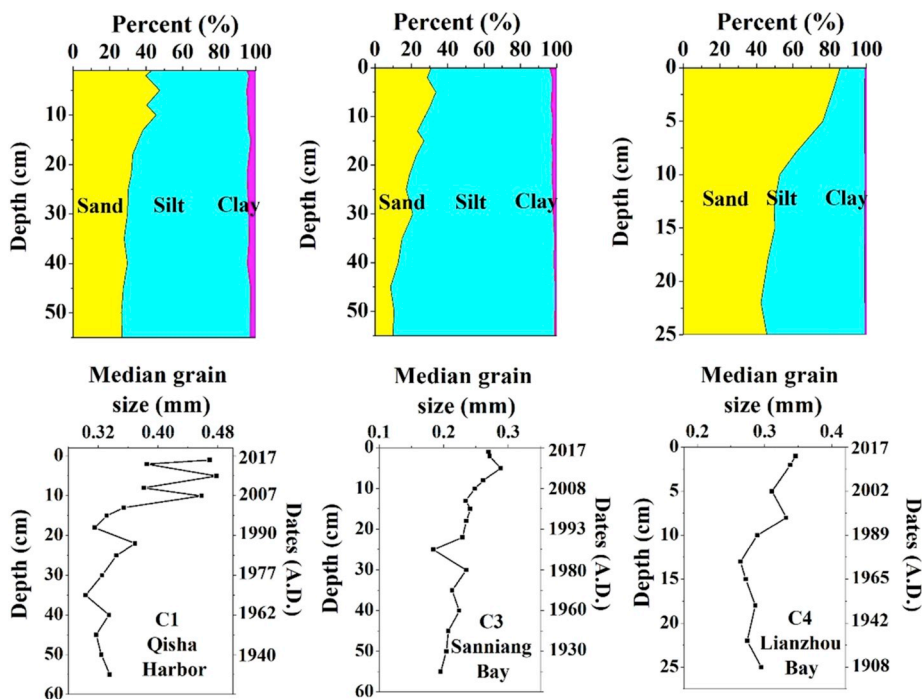


Fig. 6. Particle size distribution and historical changes in grain size.

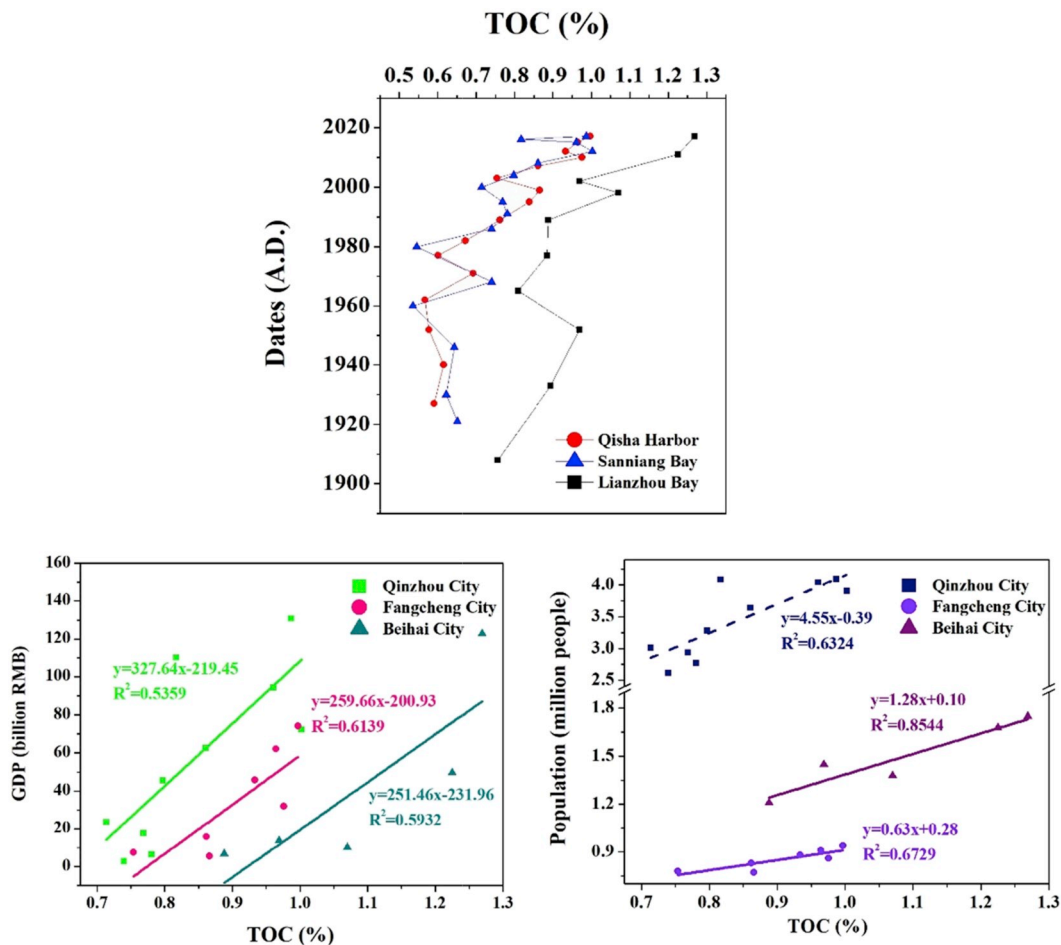


Fig. 7. Spatial and temporal distribution of TOC in the study sites and its relationship with GDP and population.

Bay, median grain size remaining stable – at around 0.27 mm – until the mid-1970s, followed by a steady increase until reaching the highest value (0.35 mm) at the top of the profile.

### 3.5. TOC concentration: spatial distribution and historical changes

TOC concentrations in sediments from the study area as well as historical changes in these concentrations are summarized in Fig. 7. In Qisha Harbor, TOC concentrations ranged between 0.57 and 1.00%. The lowest values (<0.61%) all occurred before 1970, while the highest values (>0.92%) all occurred after 2010. Plotting of the data revealed three discernible peaks in TOC concentrations at this site: the first at about 1971 (0.69%), the second at about 1999 (0.87%), and a third at about 2009 (0.97%), in addition to the highest value at the top of the profile (2017: 1.00%). All those peak TOC concentrations in Qisha Harbor were followed by a decrease in concentration varying between 4% and 12%.

In Sanniang Bay, TOC concentrations ranged between 0.54 and 1.01%. The lowest values occurred in 1960 (0.53%) and in 1980 (0.54%). A discernible peak in TOC concentration occurred between these years, in 1968 (0.74%). A second peak concentration was observed in 1991 (0.78%), and a third one in 2012 (1.01%). All those peak TOC concentrations in Sanniang Bay were followed by a decrease in concentration varying between 8% and 27%. The top six highest TOC concentrations measured at this site (>0.79%) all occurred after 2004.

Lianzhou Bay had the highest TOC concentrations among all sites and time periods, ranging from a low of 0.76% in 1908 to a high of 1.27% in 2017. Plotting of the data revealed two discernible peaks in TOC concentrations at this site: the first at about 1952 (0.97%) and the second at about 1998 (1.07%), both followed by a decrease in concentration of 16% and 10%, respectively.

Fig. 7 also shows the relationships between historical changes in TOC concentrations in sediments of the Beibu Gulf and the population and GDP growth in major cities surrounding the gulf. Results show a significant positive relationship (Pearson correlation) between historical increases in TOC concentrations and both the GDP ( $p = 0.02$ ) and population growth ( $p = 0.01$ ) on these major cities.

## 4. Discussion

In three of our four study sites,  $^{210}\text{Pb}$  activity profiles have shown to be ideal tracers for dating coastal sediments and accumulation rates over the last century. In these sites – Qisha Harbor (C1), Sanniang Bay (C3), and Lianzhou Bay (C4) – the  $^{210}\text{Pb}$  specific activity at the surface was constant and decreased exponentially or linear with cumulative sediment mass, allowing us to determine the rate of sedimentation in each site, and to use these rates to investigate natural and anthropogenic processes affecting sediment fluxes, burial, and mixing. Supported  $^{226}\text{Ra}$  concentrations were virtually constant in these cores, but  $^{210}\text{Pb}_{\text{total}}$  activity only reached radioactive equilibrium with  $^{226}\text{Ra}$  at the Lianzhou Bay site (at the 25-cm depth), suggesting slower sediment accumulation at this site (given that the equilibrium depth corresponds to about five half-lives or ca. 100 years of sediment accumulation). The resulting  $^{210}\text{Pb}_{\text{ex}}$  activity profiles for the three sites (C1, C3, C4) suggest constant sediment accumulation in steady-state conditions and limited influence from sediment mixing and changes in sedimentation rates or erosion (Arias-Ortiz et al., 2018).

Unlike the study sites discussed above, the  $^{210}\text{Pb}_{\text{ex}}$  activity profile in Maowei Sea (C2) showed a stair-stepped pattern. This irregular distribution with scattered  $^{210}\text{Pb}_{\text{ex}}$  specific activities can be caused by: (1) the deposition of  $^{210}\text{Pb}_{\text{ex}}$  outpacing its decay (Alongi et al., 2005), (2) intense sediment reworking through disturbance (Serrano et al., 2016) or by (3) a heterogeneous grain size sediment distribution with depth (Sanders et al., 2010). In our case, the irregular activity profile at site C2 may have two possible causes. First, it is likely the result of varying  $^{210}\text{Pb}_{\text{ex}}$  fluxes over time associated with sediment disturbance caused by

major changes in land use and vegetation cover during the 20th century (Ahrends et al., 2017; Hu et al., 2019). In addition, vertical mixing of sediment caused by biological and/or physical activity within the sediment column is likely contributing to the observed  $^{210}\text{Pb}_{\text{ex}}$  activity profile, mostly as a result of the intensive mariculture activities taking place in the area. This coastal bay is well known for its well-developed fish, shrimp, and shellfish aquaculture (Gu et al., 2015). During the fishing and cultivation processes, frequent mooring and refloating activities may cause significant disturbance to sediments and lead to vertical remixing of sediments. Additionally, some bioturbation may also be taking place and can result in vertical redistribution of sediments. Flooding events – which can produce an acceleration of sedimentation events (Chanton et al., 1983; Kirchner and Ehlers, 1998; Omengo et al., 2016) – may also play a role, since Maowei Sea is a semi-closed coastal embayment receiving drainage from two of the five major rivers in the Guangxi coastal region. Therefore, this sediment core is likely unavailable to establish chronology.

$^{137}\text{Cs}$  activity in Maowei Sea (which increased towards the top of the profile) also suggests continuous input of  $^{137}\text{Cs}$  from the catchment through increased soil erosion, since this nuclide is easily transported in dissolved form from upstream soils by surface runoff (Putyrskaya et al., 2009). On the other three cores (C1, C3, C4),  $^{137}\text{Cs}$  activity exhibited a distinguishable peak, suggesting that substantial mixing of the sediments had not occurred at these sites. Here, the  $^{137}\text{Cs}$  peak can be used as an independent stratigraphic chronomarker (Chen et al., 2019).

Each core showed a significant discrepancy in the chronologies estimated by the models, which has been observed in other studies (Blais et al., 1995; Von Gunten et al., 2009; Chen et al., 2019). The CRS model produced the best fit, based on support with the  $^{137}\text{Cs}$  time marker. One possible explanation for the over/under estimation of chronologies in these coastal regions during the last half century, which likely affected  $^{210}\text{Pb}_{\text{ex}}$  distribution in these sediments (Chen et al., 2019). This recycled  $^{210}\text{Pb}_{\text{ex}}$  fallout (mostly through sediment erosion) probably contributes to significant proportions of the initial  $^{210}\text{Pb}_{\text{ex}}$  inventories in the study sites, similar to what has been observed in other studies (Gaspar et al., 2013; Appleby, 2008; Tylmann et al., 2016). Since the CIC and CFCS models are greatly influenced by the initial concentrations of  $^{210}\text{Pb}$ , these models were not able to yield a reliable chronology. Conversely, the CRS model is unaffected by these changes in the initial concentrations and sedimentation rates at different layers (Appleby and Oldfield, 1978). Previous studies also suggest that, while the CIC and CFCS models have typically been used in the marine environment, the CRS model is the most preferred in lake sediments, estuarine environments and vegetated coastal ecosystems (Andersen, 2017; Breithaupt et al., 2014). Simulations undertaken by Arias-Ortiz et al. (2018) also showed that the CRS model performed better under conditions of increasing sedimentation rates, producing accumulation rates that deviated from the ideal value by less than 5%.

The  $^{210}\text{Pb}_{\text{ex}}$  redistribution in sediment from rapid urban development in the coastal regions surrounding Beibu Gulf also influenced the calculated accumulation rates in the studied sites. Relatively high sediment accumulation rates in Qisha Harbor (C1) and Sanniang Bay (C3) may be associated with their location very close to the coast, receiving a significant supply of terrigenous sediments, particularly over the last 30 years. This conclusion is supported by other studies in the region, which have found relatively high sedimentation rates in the northeastern part of Beibu Gulf, particularly in the area near the Qinzhou Bay at a water depth less than 20 m and the inner continental shelf south to Weizhou Island, west Hainan Island at a water depth between 20 m and 50 m (Xu et al., 2012; Kaiser et al., 2016). In contrast, the same authors found that pelagic sedimentation rates are low in the central part of the gulf and in offshore areas where water depth is higher than 50 m.

Overall, sediment accumulation rates remained under  $0.12 \text{ cm y}^{-1}$  before the 1970s, when human disturbance was low. After 1980,

sedimentation rates showed a steep increase (400% in C1 and 700% in C3), probably attributed to the fast pace of coastal development during that time. [Hu et al. \(2019\)](#) report that, between 1990 and 2017, a total of 4708 km<sup>2</sup> (2.0% of the total area of Guangxi Province) experienced land use transition, with the biggest losses occurring in grassland, woodland, and cropland areas. This same study shows that the municipality of Qinzhou, which is drained by three of the major rivers in the region, experienced the highest amounts of deforestation. These land changes are likely to affect flow rates in streams and rivers within the catchment areas of the studied sites. River flow or flux is indeed a key contributor to sediment accumulation increases in coastal regions, since higher river flow can produce more sediment inputs into the coast and accelerate the sedimentation process. In fact, data from a few studies done in the region ([Dai et al., 2011](#); [Li and Huang, 2018](#)) have found that flows of main rivers adjacent to sites C1 and C3 fluctuated significantly during the last 60 years, although no direct link to increased sedimentation was established. Furthermore, these studies indicated that river flows may not be the key factor to affect sedimentation, since the investigated sites are relatively far from large rivers.

[Table 2](#) compares sedimentation rates from this study and others from the literature. It also lists the depth of the water column and the distance from the shoreline for each SAR measurement. Accumulation rates over continental margins usually decrease with depth and distance from major rivers. Historical sedimentation rates in our study sites (0.06–0.79 cm y<sup>-1</sup>) are about 1.5–2 times the rates reported in offshore regions of the Beibu Gulf by [Xu et al. \(2012\)](#). Recent sedimentation rates are even higher, although they are usually within the range of those observed in impacted coastal environments (Mumbai Harbor Bay, Magra River estuary, and Bohai Sea), reflecting increased coastal sediment supply over the last 50 years. Results from the particle size analysis, which shows an increase in the proportion of sand grains since the 1990s in the study sites, also corroborate this conclusion. This shift to sandy sediments in our study area will likely mean that chronology determinations using short-lived radionuclides will become difficult since coarse sediments are often unsuitable for <sup>210</sup>Pb dating. It may lead to very low <sup>210</sup>Pb<sub>ex</sub> specific activities and to vertical remixing of <sup>210</sup>Pb in the sediment column ([Arias-Ortiz et al., 2018](#)).

TOC concentrations in our study sites have increased by about 170% over the last 100 years. Historical concentrations (before 1970) were similar to those observed offshore in the central Beibu Gulf (0.5–0.8%), which were reported by [Kaiser et al. \(2016\)](#). Current TOC concentrations in our sites range from about 0.98% (in C1 and C3) to about 1.28% (in

C4). The values measured in C1 and C3 are consistent with those reported by [Gan et al. \(2013\)](#), while our values in C4 are about 6-times higher than those reported by these authors, and about 2-times higher than those reported in the Nanliu River Estuary by [Xia et al. \(2011\)](#). Our TOC values in C4 are similar to those observed in mangrove sediments of the low intertidal region of northern Lianzhou Bay (~1.3%) which were reported by [Kaiser et al. \(2016\)](#). Our TOC concentrations are about 2–4 times higher than values reported from the Bohai Sea (Yellow Sea) in the northeastern coast of China ([Xu et al., 2018](#)), which shows TOC content at the sediment surface ranging between 0.25% (at a nearshore embayment about 10 km from the mouth of the Yellow River) to 0.72% (in the central section of the Bohai Sea). Nevertheless, our results are consistent with these and other studies reporting organic carbon content inversely proportional to distance from the coast ([Hu et al., 2009](#); [Xu et al., 2018](#)).

Previous studies have shown that riverine transport is the major source of terrestrial organic materials to the inner shelves worldwide ([Prah et al., 1994](#); [Bianchi, 2011](#); [Bouchez et al., 2014](#); [Smith et al., 2015](#); [Cui et al., 2016](#)). The same appears to be the case in our study area, where seasonality has a significant impact on carbon and nitrogen supply from these coastal rivers, and where sub-seasonal meteorological events and tides dominate temporal variability of nutrient delivery in this section of the Beibu Gulf ([Kaiser et al., 2014](#)). This is particularly true in the fluxes of dissolved fractions of these nutrients (DIN, DOC), suggesting a significant contribution of inorganic fertilizer inputs from the agricultural hinterland.

Although it was not an objective of this study to evaluate the impacts of fish stocks on carbon fluxes, fish have been shown to significantly affect biogeochemical cycling in lakes through trophic cascades ([Carpenter et al., 1985](#)), and it has previously been argued that similar processes may occur to a lesser, but perhaps still significant degree in the ocean ([Hessen and Kaartvedt, 2014](#)). To our knowledge, only one study ([Kavanagh and Galbraith, 2018](#)) have explored this relationship between fish populations and ocean carbon biogeochemistry. They compiled published records of fish abundance and compared them with biogeochemical proxy measurements. They have found both positive and negative correlations between TOC and fish abundance. In the Beibu Gulf, previous study found that the abundance of fish species with long life span, large size and high trophic levels decreased, while short-lived and small-sized fish species in low trophic levels increased their abundance over the time ([Wang et al., 2012](#)). Further exploration is needed to evaluate the impacts of this change in the community structure on

**Table 2**  
Sedimentation rates in the study area and comparable coastal regions.

Location	Model	Chronology	SAR (cm yr <sup>-1</sup> )	Depth (m)	Distance (km)	Reference
Qisha Harbor, Beibu Gulf	CRS	1927–2017	0.09–0.43	6.2	<2	This study
Sanniang Bay, Beibu Gulf		1921–2017	0.09–0.79	5.6	2.3	
Lianzhou Bay, Beibu Gulf		1908–2017	0.06–0.17	4.3	7.5	
Southern Weizhou Island, Beibu Gulf	CIC	–	0.30–0.53	28.4	68	<a href="#">Xu et al. (2012)</a>
Western Qiongzhou Strait, Beibu Gulf		–	0.10–0.49	24	46	
Northwestern Hainan Island, Beibu Gulf		–	0.50–0.53	39	31	
Central Beibu Gulf		–	0.20–0.34	37	64	
Nanliu River Estuary, Beibu Gulf	CIC	1954–2008	0.85	<5	<2	<a href="#">Gan et al. (2013)</a>
Nanliu River Estuary, Beibu Gulf	CIC	1960–2010	0.70	<5	<2	<a href="#">Kaiser et al. (2016)</a>
Laizhou Bay, Bohai Sea (Yellow Sea)	CRS	1933–2011	0.73–0.87	9	12	<a href="#">Xu et al. (2018)</a>
Liaodong Bay, Bohai Sea (Yellow Sea)		1933–2013	0.64	21	72	
Central Bohai Sea (Yellow Sea)		1900–2013	0.52	23	80	
Magra River Estuary (Ligurian Sea)	CFCS	–	>1.6	15	<2	<a href="#">Delbono et al. (2016)</a>
Magra River Shelf (Ligurian Sea)		–	0.3	16	5	
La Spezia Bay (Ligurian Sea)		–	1.0	11	<2	
La Spezia Shelf (Ligurian Sea)		–	0.3	64	3	
Mumbai Harbor Bay (Eastern Arabian Sea)	CRS	1934–2011	0.52–1.12	4.5–7.0	<2	<a href="#">Kumar et al. (2015)</a>
Outer Puck Bay (Baltic Sea)	CRS	1920–2008	0.16	19	9	<a href="#">Szmtykiewicz &amp; Zalewska (2014)</a>
Reda River Estuary (Baltic Sea)			0.45	<5	<2	

sediment biogeochemistry in the Beibu Gulf.

## 5. Conclusions

We used a  $^{210}\text{Pb}$ -based dating method to establish an accurate chronological framework for recent coastal sediment in northern Beibu Gulf, South China Sea. Three main models (CIC, CRS, and CFCS) were tested to determine these chronologies and CRS produced the best fit, based on the  $^{137}\text{Cs}$  support. Sedimentation rates calculated from  $^{210}\text{Pb}_{\text{ex}}$  and  $^{137}\text{Cs}$  activity profiles suggest constant sediment accumulation in steady-state conditions in most of the studied sites. Relatively high MAR and SAR in recent decades are likely the consequence of increased terrestrial input since the 1980s, resulting from the intensification of coastal development in the region during this period. Natural processes – such as terrestrial run-off, increase in water flow from the rivers, biologic activity, and climate – also play a role but many of these natural processes are experiencing significant amplification as a result of human activities. Our study has found a significant difference between SAR, MAR and coarse particle concentration before and after industrialization/urbanization. Additionally, the significant increase in MAR and SAR in coastal sediments has not been observed in pelagic sediments, highlighting the role that human disturbance has played in coastal sedimentation processes. We have also found a significant positive relationship between TOC and GDP/population density over the last century, another indication of the contribution of human activity to the observed increases in sediment carbon. All this is consistent with other works in the region and elsewhere that implicates human activities as the main driver of changes in the biogeochemistry of coastal sediments.

## Acknowledgments

This research was supported by the National Natural Science Foundation of China (41673105), Science and Technology Major Project of Guangxi (AA17202020).

## References

- Ahrends, A., Hollingsworth, P.M., Beckschafer, P., Chen, H., Zomer, R.J., Zhang, L., Wang, M., Xu, J., 2017. China's fight to halt tree cover loss. *Proc. R. Soc. Biol. Sci.* 284, 20162559.
- Alongi, D.M., Pfützner, J., Trott, L.A., Tirendi, F., Dixon, P., Klumpp, D.W., 2005. Rapid sediment accumulation and microbial mineralization in forests of the mangrove *Kandelia candel* in the Jiulongjiang Estuary, China. *Estuar. Coast Shelf Sci.* 63, 605–618.
- Andersen, T.J., 2017. Some practical considerations regarding the application of  $^{210}\text{Pb}$  and  $^{137}\text{Cs}$  dating to estuarine sediments. In: Weckström, K., Saunders, K., Gell, P. (Eds.), *Applications of Paleoenvironmental Techniques in Estuarine Studies*, Skilbeck, C., Springer, Dordrecht, pp. 121–140pp.
- Appleby, P.G., 2001. Chronostratigraphic techniques in recent sediments. In: Last, W.M., Smol, P. (Eds.), *Tracking Environmental Change Using Lake Sediments. Basin Analysis, Coring, and Chronological Techniques*, vol. 1. Kluwer Academic Publishers, Dordrecht, pp. 171–203.
- Appleby, P.G., 2008. Three decades of dating recent sediments by fallout radionuclides: a review. *Holocene* 18, 83–93.
- Appleby, P.G., Oldfield, F., 1978. The calculation of  $^{210}\text{Pb}$  dates assuming a constant rate of supply of unsupported  $^{210}\text{Pb}$  to the sediment. *Catena* 5, 1–8.
- Appleby, P.G., Oldfield, F., 1983. The assessment of  $^{210}\text{Pb}$  data from sites with varying sediment accumulation rates. *Hydrobiologia* 103, 29–35.
- Arias-Ortiz, A., Masqué, P., Garcia-Orellana, J., Serrano, O., Mazarrasa, I., Marbà, N., Lovelock, C.E., Lavery, P.S., Duarte, C.M., 2018. Reviews and syntheses:  $^{210}\text{Pb}$ -derived sediment and carbon accumulation rates in vegetated coastal ecosystems—setting the record straight. *Biogeosciences* 15, 6791–6818.
- Begy, R.C., Simon, H., Kelemen, S., Preoteasa, L., 2018. Investigation of sedimentation rates and sediment dynamics in Danube Delta lake system (Romania) by  $^{210}\text{Pb}$  dating method. *J. Environ. Radioact.* 192, 95–104.
- Bianchi, T.S., 2011. The role of terrestrially derived organic carbon in the coastal ocean: a changing paradigm and the priming effect. *Proc. Natl. Acad. Sci.* 108, 19473–19481.
- Blais, J.M., Kalff, J., Cornett, R.J., Evans, R.D., 1995. Evaluation of  $^{210}\text{Pb}$  dating in lake sediments using stable Pb, *Ambrosia* pollen, and  $^{137}\text{Cs}$ . *J. Paleolimnol.* 13, 169–178.
- Bouchez, J., Galv, V., Hilton, R.G., Gaillardet, J., Moreira-Turcq, P., Pérez, M.A., France-Lanord, C., Maurice, L., 2014. Source, transport and fluxes of Amazon River particulate organic carbon: insights from river sediment depth-profiles. *Geochem. Cosmochim. Acta* 133, 280–298.
- Breithaupt, J.L., Smoak, J.M., Smith, T.J., Sanders, C.J., 2014. Temporal variability of carbon and nutrient burial, sediment accretion, and mass accumulation over the past century in a carbonate platform mangrove forest of the Florida Everglades. *J. Geophys. Res. Biogeophys.* 119, 2032–2048.
- Carpenter, S., Kitchell, J., Hodgson, J., 1985. Cascading trophic interactions and lake productivity. *Bioscience* 35 (10), 634–639.
- Chanton, J.P., Martens, C.S., Kipphut, G.W., 1983. Lead-210 sediment geochronology in a changing coastal environment. *Geochem. Cosmochim. Acta* 47, 1791–1804.
- Chen, X., Qiao, Q., McGowan, S., Zeng, L.H., Stevenson, M.A., Xu, L., Huang, C.L., Liang, J., Cao, Y.M., 2019. Determination of geochronology and sedimentation rates of shallow lakes in the middle Yangtze reaches using  $^{210}\text{Pb}$ ,  $^{137}\text{Cs}$  and spheroidal carbonaceous particles. *Catena* 174, 546–556.
- Chen, Z.Z., Xu, S.N., Qiu, Y.S., Lin, Z.J., Jia, X.P., 2009. Modeling the effects of fishery management and marine protected areas on the Beibu Gulf using spatial ecosystem simulation. *Fish. Res.* 100, 222–229.
- Corcoran, M., Sherif, M.I., Smalley, C., Li, A., Rockne, K.J., Giesy, J.P., Sturchio, N.C., 2018. Accumulation rates, focusing factors, and chronologies from depth profiles of  $^{210}\text{Pb}$  and  $^{137}\text{Cs}$  in sediments of the Laurentian Great Lakes. *J. Great Lakes Res.* 44, 693–704.
- Crozaz, G., Picciotto, E., De Breuck, W., 1964. Antarctic snow chronology with Pb210. *J. Geophys. Res.* 69, 2597–2604.
- Cui, X., Bianchi, T.S., Savage, C., Smith, R.W., 2016. Organic carbon burial in fjords: terrestrial versus marine inputs. *Earth Planet. Sci. Lett.* 451, 41–50.
- Dai, J.F., Zhang, X.H., Wang, D.Q., Guo, C.Q., Ye, F., Fang, R.J., 2011. Analysis of distribution regulation of river flow discharge into Beibu gulf economic region. *Water Resour. Power* (2), 4–6, 2011.
- Delbono, I., Barsanti, M., Schirone, A., Conte, F., Delfanti, R., 2016.  $^{210}\text{Pb}$  mass accumulation rates in the depositional area of the Magra River (Mediterranean Sea, Italy). *Cont. Shelf Res.* 124, 35–48.
- Di Gregorio, D.E., Fernández Niello, J.O., Huck, H., Somacal, H., Curutchet, G., 2007.  $^{210}\text{Pb}$  dating of sediments in a heavily contaminated drainage channel to the La Plata estuary in Buenos Aires, Argentina. *Appl. Radiat. Isot.* 65, 126–130.
- Egorov, V.N., Povinec, P.P., Polikarpov, G.G., Stokozov, N.A., Gulín, S.B., Kulebakina, L. G., Osvath, I., 1999. Sr-90 and Cs-137 in the Black Sea after the Chernobyl NPP accident: inventories, balance and tracer applications. *J. Environ. Radioact.* 43, 137–155, 491.
- Gan, H., Lin, J., Liang, K., Xia, Z., 2013. Selected trace metals (As, Cd and Hg) distribution and contamination in the coastal wetland sediment of the northern Beibu Gulf, South China Sea. *Mar. Pollut. Bull.* 66, 252–258.
- Gaspar, L., Navas, A., Walling, D.E., Machín, J., Gómez Arozamena, J., 2013. Using  $^{137}\text{Cs}$  and  $^{210}\text{Pb}_{\text{ex}}$  to assess soil redistribution on slopes at different temporal scales. *Catena* 102, 46–54.
- Gu, Y.G., Lin, Q., Yu, Z.L., Wang, X.N., Ke, C.L., Ning, J.J., 2015. Speciation and risk of heavy metals in sediments and human health implications of heavy metals in edible nekton in Beibu Gulf, China: a case study of Qinzhou Bay. *Mar. Pollut. Bull.* 101, 852–859.
- Hessen, D., Kaartvedt, S., 2014. Top-down cascades in lakes and oceans: different perspectives but same story? *J. Plankton Res.* 36 (4), 914–924.
- Hu, L., Guo, Z., Feng, J., Yang, Z., Fang, M., 2009. Distributions and sources of bulk organic matter and aliphatic hydrocarbons in surface sediments of the Bohai Sea, China. *Mar. Chem.* 113, 197–211.
- Hu, Y., Batunacun, Zhen, L., Zhuang, D., 2019. Assessment of land-use and land-cover change in Guangxi, China. *Sci. Rep.* 9, 2189.
- Kaiser, D., Unger, D., Qiu, G., Zhou, H., Gan, H., 2013. Natural and human influences on nutrient transport through a small subtropical Chinese estuary. *Sci. Total Environ.* 450, 92–107.
- Kaiser, D., Unger, D., Qiu, G., 2014. Particulate organic matter dynamics in coastal systems of the northern Beibu Gulf. *Cont. Shelf Res.* 82, 99–118.
- Kaiser, D., Schulz-Bull, D.E., Waniek, J.J., 2016. Profiles and inventories of organic pollutants in sediments from the central Beibu Gulf and its coastal mangroves. *Chemosphere* 153, 39–47.
- Kavanagh, L., Galbraith, E., 2018. Links between fish abundance and ocean biogeochemistry as recorded in marine sediments. *PLoS One* 13 (8), e0199420.
- Kirchner, G., 2011.  $^{210}\text{Pb}$  as a tool for establishing sediment chronologies: examples of potentials and limitations of conventional dating models. *J. Environ. Radioact.* 102, 490–494.
- Kirchner, G., Ehlers, H., 1998. Sediment geochronology in changing coastal environments: potentials and limitations of the  $^{137}\text{Cs}$  and  $^{210}\text{Pb}$  methods. *J. Coast. Res.* 14, 483–492.
- Klaminder, J., Appleby, P., Crook, P., Renberg, I., 2012. Post-deposition diffusion of  $^{137}\text{Cs}$  in lake sediment: implications for radiocaesium dating. *Sedimentology* 59, 2259–2266.
- Koide, M., Soutar, A., Goldberg, E.D., 1972. Marine geochronology with  $^{210}\text{Pb}$ . *Earth Planet. Sci. Lett.* 14, 442–446.
- Kumar, B., Rai, S.P., Nachiappan, R.P., Kumar, U.S., Singh, S., Diwedi, V.K., 2007. Sedimentation rate in North Indian lakes estimated using  $^{137}\text{Cs}$  and  $^{210}\text{Pb}$  dating techniques. *Curr. Sci.* 92, 10.
- Kumar, A., Rout, S., Karpe, R., Mishra, M.K., Narayanan, U., Ravi, P.M., Singhal, R.K., Ravi, P.M., Tripathi, R.M., 2015. Inventory, fluxes and residence times from the depth profiles of naturally occurring  $^{210}\text{Pb}$  in marine sediments of Mumbai Harbor Bay. *Environ. Earth Sci.* 73, 4019–4031.
- Li, P.Y., Xue, R., Wang, Y.H., Zhang, R.J., Zhang, G., 2015. Influence of anthropogenic activities on PAHs in sediments in a significant gulf of low-latitude developing regions, the Beibu Gulf, South China Sea: distribution, sources, inventory and probability risk. *Mar. Pollut. Bull.* 90, 218–226.

- Li, S.S., Huang, H., 2018. Variations of runoff and sediment in Qinjiang River in the past 50 year. *Guangxi Sci.* 25, 409–417.
- Lin, W.H., Yu, K.F., Wang, Y.H., Liu, X.M., Ning, Q.Y., Huang, X.Y., 2019. Radioactive level of coral reefs in the South China Sea. *Mar. Pollut. Bull.* 142, 43–53.
- Lüder, B., Kirchner, G., Lücke, A., Zolitschka, B., 2006. Palaeoenvironmental reconstructions based on geochemical parameters from annually laminated sediments of Sacrower See (northeastern Germany) since the 17th century. *J. Palaeolimnol.* 35, 897–912.
- Ma, F., Wang, Y., Li, Y., Ye, C., Xu, Z., Zhang, F., 2010. The application of geostatistics in grain size trend analysis: a case study of eastern Beibu Gulf. *Acta Geograph. Sin.* 20, 77–90.
- Mahmood, Z.U.W., Ishak, A.K., Bakar, N.S.A., Ishak, K., Mohamed, C.A.R., 2011. Vertical distribution of  $^{210}\text{Pb}$  and  $^{226}\text{Ra}$  and their activity ratio in marine sediment core of the East Malaysia coastal waters. *J. Radioanal. Nucl. Chem.* 289, 953–959.
- Mook, W.G., 2001. Environmental isotopes in the hydrological cycle: principles and applications. [http://www.naweb.iaea.org/naweb/ih/IHS\\_resources\\_publication\\_hydroCycle\\_en.html](http://www.naweb.iaea.org/naweb/ih/IHS_resources_publication_hydroCycle_en.html)IAEA-UNESCO.
- Oldfield, F., Wake, R., Boyle, J., Jones, R., Nolan, S., Gibbs, Z., Appleby, P., Fisher, E., Wolff, G., 2003. The late-Holocene history of Gormire Lake (NE England) and its catchment: a multiproxy reconstruction of past human impact. *Holocene* 13, 677–690.
- Omengo, F.O., Alleman, T., Geeraert, N., Bouilloon, S., Govers, G., 2016. Sediment deposition patterns in a tropical floodplain, Tana River, Kenya. *Catena* 143, 57–69.
- Pan, C.G., Yu, K.F., Wang, Y.H., Zhang, W., Zhang, J., Guo, J., 2019. Perfluoroalkyl substances in the riverine and coastal water of the Beibu Gulf, South China: spatiotemporal distribution and source identification. *Sci. Total Environ.* 660, 297–305.
- Prahl, F.G., Ertel, J.R., Goñi, M.A., Sparrow, M.A., Eversmeyer, B., 1994. Terrestrial organic carbon contributions to sediments on the Washington margin. *Geochem. Cosmochim. Acta* 58, 3035–3048.
- Putyrskaya, V., Klemm, E., Röhlén, S., 2009. Migration of  $^{137}\text{Cs}$  in tributaries, lake water and sediment of Lago Maggiore (Italy, Switzerland)—analysis and comparison with Lago di Lugano and other lakes. *J. Environ. Radioact.* 100, 35–48.
- Robbins, J.A., Edgington, D.N., 1975. Determination of recent sedimentation rates in Lake Michigan using Pb-210 and Cs-137. *Geochem. Cosmochim. Acta* 39, 285–304.
- Sanchez-Cabeza, J.A., Ruiz-Fernández, A.C., 2012.  $^{210}\text{Pb}$  sediment radiochronology: an integrated formulation and classification of dating models. *Geochem. Cosmochim. Acta* 82, 183–200.
- Sanders, C.J., Santos, I.R., Silva-Filho, E.V., Patchineelam, S.R., 2006. Mercury flux to estuarine sediments, derived from Pb-210 and Cs-137 geochronologies (Guaratuba Bay, Brazil). *Mar. Pollut. Bull.* 52, 1085–1089.
- Sanders, C.J., Smoak, J.M., Sanders, L.M., Waters, M.N., Patchineelam, S.R., Ketterer, M.E., 2010. Intertidal mangrove mudflat  $^{240+239}\text{Pu}$  signatures, confirming a  $^{210}\text{Pb}$  geochronology on the southeastern coast of Brazil. *J. Radioanal. Nucl. Chem.* 283, 593–596.
- Sarı, E., Çagatay, M.N., Acar, D., Belivermiş, M., Kılıç, Ö., Arslan, T.N., Tutay, A., Kurt, M.A., Sezer, N., 2018. Geochronology and sources of heavy metal pollution in sediments of Istanbul Strait (Bosporus) outlet area, SW Black Sea, Turkey. *Chemosphere* 205, 387–395.
- Serrano, O., Ruhon, R., Lavery, P.S., Kendrick, G.A., Hickey, S., Masqué, P., Arias-Ortiz, A., Steven, A., Duarte, C.M., 2016. Impact of mooring activities on carbon stocks in seagrass meadows. *Sci. Rep.* 6, 23193.
- Smith, J.N., 2001. Why should we believe  $^{210}\text{Pb}$  sediment geochronologies? *J. Environ. Radioact.* 55, 121–123.
- Smith, R.W., Bianchi, T.S., Allison, M., Savage, C., Galy, V., 2015. High rates of organic carbon burial in fjord sediments globally. *Nat. Geosci.* 8, 450–453.
- Smol, J.P., 2008. *Pollution of Lakes and Rivers: A Paleoenvironmental Perspective*, second ed. Blackwell Publishing, Malden, MA.
- Szmytkiewicz, A., Zalewska, T., 2014. Sediment deposition and accumulation rates determined by sediment trap and  $^{210}\text{Pb}$  isotope methods in the Outer Puck Bay (Baltic Sea). *Oceanologia* 56, 85–106.
- Tee, L.T., Ahmad, Z., Mohamed, C.A.R., 2003. Estimation of sedimentation rates using  $^{210}\text{Pb}$  and  $^{210}\text{Po}$  at the coastal water of Sabah, Malaysia. *J. Radioanal. Nucl. Chem.* 256, 115–120.
- Tylmann, W., Bonk, A., Goslar, T., Wulf, S., Grosjean, M., 2016. Calibrating  $^{210}\text{Pb}$  dating results with varve chronology and independent chronostratigraphic markers: problems and implications. *Quat. Geochronol.* 32, 1–10.
- Venunathan, N., Narayana, Y., 2016. Activity of  $^{210}\text{Po}$  and  $^{210}\text{Pb}$  in the riverine environs of coastal Kerala on the southwest coast of India. *J. Radiat. Res. Appl. Sci.* 9, 392–399.
- Von Gunten, L., Grosjean, M., Beer, J., Grob, P., Morales, A., Urrutia, R., 2009. Age modeling of young non-varved lake sediments: methods and limits. Examples from two lakes in Central Chile. *J. Paleolimnol.* 42, 401–412.
- Wang, X., Qiu, Y., Du, F., Lin, Z., Sun, D., Huang, S., 2012. The variation trend of fish diversity and dominant species in the bottom of Beibu Gulf in autumn. *Acta Ecol. Sin.* 32 (2), 333–342.
- Xia, P., Meng, X., Yin, P., Cao, Z., Wang, X., 2011. Eighty-year sedimentary record of heavy metal inputs in the intertidal sediments from the Nanliu River estuary, Beibu Gulf of South China Sea. *Environ. Pollut.* 159, 92–99.
- Xu, D., Chu, F., Yang, H., Chen, L., Li, T., 2012. Modern sedimentation rates in the Beibu gulf. *Mar. Geol. Quat. Geol.* 32, 17–26.
- Xu, Y., Zhou, S., Hu, L., Wang, Y., Xiao, W., 2018. Different controls on sedimentary organic carbon in the Bohai Sea: river mouth relocation, turbidity and eutrophication. *J. Mar. Syst.* 180, 1–8.